



## Electrostatic attachment of exosome onto a 3D-fabricated calcium silicate/polycaprolactone for enhanced bone regeneration

Ju Hyun Yun<sup>a</sup>, Hye-Young Lee<sup>b</sup>, Se Hyun Yeou<sup>b</sup>, Jeon Yeob Jang<sup>b</sup>, Chul-Ho Kim<sup>b</sup>, Yoo Seob Shin<sup>b,c,\*</sup>, Darryl D. D'Lima<sup>c</sup>

<sup>a</sup> Department of Otorhinolaryngology-Head and Neck Surgery, College of Medicine, Ewha Womans University, Seoul, 07985, Republic of Korea

<sup>b</sup> Department of Otolaryngology, School of Medicine, Ajou University, Suwon, 16499, Republic of Korea

<sup>c</sup> Scripps Health, Shiley Center for Orthopedic Research and Education at Scripps Clinic, La Jolla, CA, 92121, USA

### ARTICLE INFO

#### Keywords:

3D fabrication  
Bone regeneration  
Calcium silicate  
Electrostatics  
Exosome

### ABSTRACT

Exosomes have garnered attention for use in bone regeneration, but their low activity, rapid degradation, and inaccurate delivery have been obstacles to their use in clinical applications. As such, there exists a need for an exosome-integrated delivery platform. Calcium silicate (Ca-Si) is considered one of the most promising bio-ceramics for bone regeneration because of its remarkable ability to promote hydroxyapatite formation, osteoblast proliferation, and differentiation. However, Ca-Si has limitations, such as a high degradation rate leading to high pH values. Here, we propose a bone regeneration platform: three-dimensional-fabricated Ca-Si scaffolds immersed in polycaprolactone (PCL) coated with exosomes. This setup enhanced porosity, mechanical strength, and natural hydroxyapatite formation. Ca-Si incorporation increased the quantity of attached exosomes on the scaffold and enabled more sustainable control of their release compared to bare PCL. The exosome-coated scaffold exhibited excellent cell attachment and osteogenic differentiation, significantly increasing biocompatibility and the *in situ* recruitment of stem cells when transplanted into the subcutaneous tissue of mice. The bone regenerating efficacy of the exosome-attached scaffold was confirmed using a mouse calvarial bone defect animal model. These findings suggest a potential application of exosome-coated Ca-Si/PCL scaffolds as an osteogenic platform for critical bone defects.

### 1. Introduction

A critical size defect (CSD) refers to the minimum size of a bone injury that cannot be healed by the natural spontaneous regeneration of the body [1,2]. A variety of bone substitutes have been used to reconstruct bone damage that exceeds the CSD. Autologous or allogeneic bone transplants can be viable clinical options for repairing bone defects [3, 4], but they come with the drawbacks of increased surgical time, additional scars, donor site morbidity, and the risk of disease transmission and rejection. Other synthetic bone substitutes, such as hydroxyapatite (HA), calcium phosphate cements, or bioactive glasses, are also utilized in clinical settings [5]. These materials also have significant limitations, including undesirable mechanical properties [6,7]. Therefore, extensive research is underway to find biomaterials that maximize the benefits of existing bone substitutes and address their limitations [8–11].

Recently, mesenchymal stem cell (MSC)-derived exosomes have

been considered a promising therapeutic material for bone regeneration [12]. Exosomes are lipid bilayer-enclosed extracellular vesicles that carry various proteins, RNA, and bioactive molecules depending on their parent cells, and their contents are closely related to their parent cells' origin [13–15]. MSC, which are multipotent stem cells capable of differentiating into various cell types, including osteocytes and osteoblasts, promotes bone generation [16]. However, the administration of live cells carries potential safety risks, such as microvasculature occlusion. Therefore, MSC-derived exosomes, which retain the characteristics of stem cells, might be a safer alternative [17]. While their natural targeting accuracy may not always suffice for delivering designated cargos to specific recipient cells, this can be optimized by manipulating exosomes, potentially broadening their clinical applications, including bone regeneration [12,18]. In light of this, we designed three-dimensional (3D)-molded scaffolds based on calcium silicate (Ca-Si) and polycaprolactone (PCL) to optimize the 3D distribution of exosomes and

\* Corresponding author. Department of Otolaryngology, Ajou University School of Medicine, 164 World-Cup Street, Yeongtong-gu, Suwon, 16499, Republic of Korea.

E-mail address: [ysshinmd@ajou.ac.kr](mailto:ysshinmd@ajou.ac.kr) (Y.S. Shin).

<https://doi.org/10.1016/j.mtbio.2024.101283>

Received 21 July 2024; Received in revised form 20 September 2024; Accepted 30 September 2024

Available online 1 October 2024

2590-0064/© 2024 The Authors. Published by Elsevier Ltd. This is an open access article under the CC BY-NC license (<http://creativecommons.org/licenses/by-nc/4.0/>).

adapt to irregular bone defects.

Ca-Si-based biomaterials are being evaluated as promising alternatives for bone regeneration due to their bioactive properties [9]. They can interact with the surrounding biological environment and promote the formation of HA, which is a mineral component of natural bone [19, 20]. Furthermore, the release of silicate ions promotes osteogenic differentiation and angiogenesis, providing a suitable scaffold for stem cells so that they can proliferate and regenerate new bone tissue [21,22]. However, the brittle and weak mechanical characteristics of Ca-Si-based biomaterials, as well as their rapid degradation, which results in high pH values, hinder their use for treatment of CSDs [23–25]. Recent studies have concentrated on improving the dissolution rate, apatite-forming capability, and biological performance of Ca-Si ceramics to make them more suitable for bone tissue engineering. This has been accomplished through several different synthetic approaches, including the incorporation of different elements such as magnesium, zinc, or zirconium [9]. We hypothesized that the addition of PCL and exosome coating could help Ca-Si-based biomaterials to maintain the mechanical strength until bone regeneration is complete.

In this investigation, we developed a novel bone-regenerating platform: 3D-fabricated Ca-Si scaffolds immersed in PCL solution and coated with exosomes, which could enhance the strength of each material and mitigate their drawbacks. Structural analyses and mechanical testing of the scaffolds were performed based on the incorporation of Ca-Si into the PCL strands. The attachment and release pattern of the exosomes from the scaffolds was evaluated. Improvements of cell viability, migration, differentiation, and extracellular matrix (ECM) production were investigated both *in vitro* and *in vivo*. The *in vivo* bone-regenerating ability of the scaffold was evaluated using a mouse calvarial bone defect animal model. The aim of this study was to evaluate the potential of exosome-coated Ca-Si/PCL scaffolds as a novel osteogenic platform for critical bone defects.

## 2. Materials and methods

### 2.1. 3D molded Ca-Si/PCL composite scaffold formed by thermally induced phase separation

The 3D porous scaffolds were fabricated using thermally induced phase separation with a 3D-fabricated polyvinyl alcohol (PVA) mold. The PVA mold was designed by computer-aided design software (AutoCAD®, Autodesk, Inc., USA) and fabricated with Zortrax M200 PLUS (Zortrax, Poland). For the printing process, high quality and maximum infill settings were chosen. Other parameters were automatically set to the optimal values recommended by Zortrax for the specific water-soluble PVA filament (diameter: 1.75 mm, e-SUN, China) being used. The casting mold was printed with water soluble PVA filament (diameter: 1.75 mm, e-SUN, China). The mold was created using a 3D fabrication process. Four layers of 700 μm diameter fibers were printed with 500 μm inter-fiber spacing. The layers were printed at a 30° angle to each other, resulting in a final scaffold with a height of 2 mm and a diameter of 14 mm.

Mixtures of PCL and CaSiO<sub>3</sub> (10 and 20 % of the mass of the PCL) were dissolved in a dioxane:water (9:1) solution. The uniformly mixed Ca-Si/PCL solution was injected into a PVA mold using a syringe, immersed in -20 °C pre-cooled ethanol, and stored in a freezer. After 16 h, the PVA molds were transferred in the cold ethanol to a refrigerator and stored for 72 h. The ethanol was changed every 24 h to extract the dioxane. After the extraction process, the PVA mold was dissolved in deionized water and dried completely.

### 2.2. Characterizations of porous Ca-Si/PCL composite scaffolds

#### 2.2.1. Morphological characterization

The morphology and microstructure of the scaffolds were analyzed with field emission scanning electron microscopy (SEM, JEOL JSM-

7900F, Japan) at 5 kV, and the elemental content of the scaffolds was quantitatively analyzed with energy dispersive X-ray spectrometry (EDX, JEOL JSM-7900F, Japan).

#### 2.2.2. Fourier-transform infrared spectroscopy (FTIR)

The PCL scaffolds were measured with FTIR (Nicolet 5DXC spectrometer, Thermo Fisher Scientific, USA) using attenuated total reflection. Spectra were recorded from 4000 to 400 cm<sup>-1</sup> with a resolution of 4 cm<sup>-1</sup> and a scan frequency of 32 times in transmission mode.

#### 2.2.3. X-ray diffraction (XRD)

XRD patterns were recorded with a multipurpose X-ray diffractometer (SmartLab, Rigaku, Japan) using a Cu target. The XRD patterns of the scaffolds were recorded over a 2θ range 20°–70° and the scan speed was set to 3°/min.

#### 2.2.4. Mechanical properties

Compressive mechanical properties were characterized at room temperature using a ProLine Z005 universal test machine (Zwick-Roell, Ulm, Germany). A set of 5 cylindrical samples (diameter × height: 14 × 10 mm<sup>2</sup>) was compressed at 2 mm/min to a strain level of ~50 %.

#### 2.2.5. Porosity of the 3D-fabricated scaffold

The porosity (ε) of the scaffold was calculated based on the volume-dependent density of the 3D scaffold. First, the volume (A) of a 3D scaffold with a known mass (m) was measured so that the density (ρ<sub>0</sub>) of the scaffold could be calculated with

$$\rho_0 = \frac{m}{A}$$

The value of ε was determined from the ratio of the density of the material (ρ) to ρ<sub>0</sub>:

$$\varepsilon = \left(1 - \frac{\rho}{\rho_0}\right) \times 100\%$$

#### 2.2.6. In vitro degradation and ion release

Four groups of scaffolds with weight  $W_0$  were immersed in phosphate-buffered saline (PBS) at 37 °C with constant shaking for 28 days to assess the degradation rate *in vitro*. The ratio of PBS volume to  $W_0$  was 0.025 g/mL. Aliquots of each group were removed after 1, 4, 7, 10, 14, 21, and 28 days; gently washed with deionized water; dried at room temperature; and weighed to determine their weight at time  $t$  ( $W_t$ ). The percentage of scaffold weight loss ( $W_r$ ) was calculated as

$$W_r = \frac{W_0 - W_t}{W_0} \times 100\%$$

The release of Si<sup>+</sup> ions was measured in triplicate after 1, 3, 7, 14, and 21 days of immersion. The ion concentrations of the scaffolds were measured by inductively coupled plasma optical emission spectrometry (ICP-OES, iCAP PRO XP DUO, Thermo Fisher, USA), and the pH values were detected with a pH meter (Beckman Φ-310 pH meter, Beckman Instruments, CA) at the predetermined time points.

### 2.3. Isolation and identification of osteogenic-induced tonsil-derived mesenchymal stem cell (TMSC)-derived exosomes

#### 2.3.1. Preparation and osteogenic differentiation of human tonsil-derived mesenchymal stem cells (hTMSCs)

Human tonsil-derived mesenchymal stem cells (hTMSCs) were isolated from human tonsil tissue obtained from the department of otolaryngology in Ajou University Hospital (Suwon, Korea). This study was approved by the Institutional Review Board (IRB) of Ajou University Hospital (AJIRB-BMR-SMP-17-494) and all procedures were performed in accordance with relevant regulations. First, the tonsil tissue was washed three times with phosphate-buffered saline (PBS, Welgene, Korea) containing 4 % antibiotic-antimycotic solution. After washing,

the tonsil tissue was cut into small pieces using a surgical scalpel. The tissue was then digested with a 0.075 % collagenase type-I (Worthington, USA) solution for 30 min at 37 °C. To neutralize the collagenase activity, the digested tissue was mixed with Dulbecco Modified Eagle Medium (DMEM, Welgene, Korea) supplemented with 10 % fetal bovine serum (FBS, Gibco, USA) and 1 % antibiotic-antimycotic solution (Gibco). The mixture was then filtered through a 40 µm cell strainer (BD Falcon, USA) to remove cellular debris. The cell suspension was centrifuged at 1300 rpm for 3 min. This process was repeated three times. The final cell pellet was resuspended in control media and incubated at 37 °C in a 5 % CO<sub>2</sub> environment. The cells were used for experiments up to passage five.

The cells were washed with PBS containing 1 % FBS. Cells from passage 3 were stained for 1 h on ice with fluorescein isothiocyanate (FITC)-conjugated antibodies. Stained cells were analyzed using Flow cytometry (FACS Canto II, BD Bioscience, CA, USA). FACS data were analyzed by using FlowJo software (Tree Star, USA)

To investigate the potential of hTMSCs for bone formation (osteogenic differentiation), the cells were cultured in a specialized osteogenic medium. This medium consisted of DMEM supplemented with 10 % FBS, 1 % antibiotic-antimycotic solution, 10 mM β-glycerophosphate, 50 µM L-ascorbic acid, and 100 nM dexamethasone. The cells were cultured in this medium for 2 weeks to induce osteogenic differentiation.

### 2.3.2. Isolation of osteogenic-induced TMSC-derived exosomes

Exosomes were isolated using an ExoQuick-TC ULTRA EV Isolation Kit for Tissue Culture Media (System Biosciences, CA, USA) according to the manufacturer's instructions. The TMSCs were cultured in osteogenic induction medium containing 100 nM dexamethasone, 10 mM β-glycerophosphate, and 50 µg/mL ascorbic acid in Dulbecco's modified eagle medium as a growth medium that was supplemented with 10 % fetal bovine serum (FBS, Gibco, USA) and 1 × Anti-Anti (Gibco) for 2 weeks and subsequently cultured in FBS-free medium for 48 h. For exosome isolation, TMSC-cultured materials were collected and centrifuged at 3000g for 15 min to remove cells and cell debris, and the supernatant was transferred to a new tube and mixed with ExoQuick-TC solution. The tube was gently inverted several times to mix the materials, refrigerated overnight at 4 °C, and centrifuged at 1500g for 30 min to remove the supernatant. The remaining pellet was resuspended in PBS. The concentration of exosomes was measured using a DC protein assay kit (Bio-Rad, CA, USA).

### 2.3.3. Zeta potentials of the exosome vesicles (EVs)

A zeta potential analyzer (ZetaSizer Pro, Malvern Panalytical, Malvern, UK) was used to measure the zeta potential and size of exosome isolated with the Exoquick-TC kit. Exosome was diluted with Buffer B from the kit and PBS at a ratio of 1:100 and injected into a folded capillary zeta cell (DTS1070, Malvern Panalytical, Malvern, UK) and zeta potential and dynamic light scattering analysis was performed with ZS XPLOER software (Malvern Panalytical Ltd., Malvern, UK). Measurements were made in triplicate and the average value was reported. Additionally, polydopamine (pDA)-coated exosome was incubated in 2 mg/mL dopamine hydrochloride (Sigma, USA) in 10 mM Tris HCl (pH 8.5) for 2 h at 4 °C with rotation at 1 rpm to prevent aggregation.

### 2.3.4. In vitro bioactivity analysis of scaffolds in simulated body fluid

Scaffolds were immersed in 5× SBF and incubated at 37 °C for 7 days. After incubation, the scaffolds were removed and washed with deionized water. The scaffolds were then characterized using SEM and EDS to assess their surface morphology and elemental composition.

## 2.4. In vitro assays

### 2.4.1. Synthesis of pDA-Ca-Si/PCL 3D scaffolds and bioactivity

Ca-Si/PCL 3D scaffolds were immersed in a 2 mg/mL solution of dopamine hydrochloride (Sigma, USA) in 10 mM Tris HCl (pH 8.5) for

16 h and then dried at room temperature. Exosomes were attached to Ca-Si/PCL scaffolds that had been treated with pDA by coating them with 100 µg/mL exosome solution for 2 h at 4 °C. Cells were seeded in growth medium and incubated at 37 °C in a 5 % CO<sub>2</sub> atmosphere. Cell viability and proliferation on scaffolds were evaluated using a Cell Counting Kit-8 (CCK-8, Dojindo, Japan) with four replicates (n = 4) per experimental group.

### 2.4.2. PKH26 fluorescent labeling of exosome internalization

Isolated exosomes were labelled with PKH26 (Red Fluorescent Cell linker for General Cell Membrane, Sigma-Aldrich, USA) according to the manufacturer's instructions. Briefly, exosomes were resuspended in 500 µL of diluent C, and 2 µL of the PKH26 mixture (2 µM PKH26) was incubated with exosomes for 5 min. PKH26-labelled exosomes were added to the pDA scaffold for 2h at 4 °C. After incubation, the scaffolds were washed with PBS to remove unbound dye and exosomes, and cellular uptake of the exosomes by TMSC was observed with EVOS2 fluorescence microscopy (Thermo Fisher Scientific, USA).

### 2.4.3. Boyden chamber migration assay

Ca-Si/PCL scaffolds were loaded into the lower chamber with 5 % FBS, and the TMSCs were cultured in the upper chamber (pore size: 8 µm; SPL, Korea) with FBS-free media. After 24 h of incubation, triplicate samples were collected to assess cell migration. Cells that migrated to the lower chamber were fixed with 4 % paraformaldehyde, stained with DAPI and phalloidin, and counted under an EVOS2 fluorescence microscope for quantification.

### 2.4.4. Osteogenic differentiation assays

Alkaline phosphatase (ALP) and Alizarin Red S (ARS) staining were used to evaluate the bioactivity of the scaffolds for tissue engineering and triplicate measurements were performed for each condition. The measurement of ALP activity of the TMSC-cultured scaffolds was performed by adding p-nitrophenyl phosphate (pNPP, Sigma-Aldrich, USA) to the cell lysate and hydrolyzing by the ALP enzyme. The reaction was stopped after 60 min by adding 1 N NaOH, and the results were measured spectrophotometrically at 405 nm (BioTek Instruments, USA).

Alizarin red is a calcium-binding dye that selectively stains calcium-rich deposits in an ECM. The staining protocol used 4 % paraformaldehyde for 10 min and then 0.2 % ARS for another 15 min. After staining, calcium deposition was imaged using an optical microscope.

### 2.4.5. Western blot assay

The western blot assay was performed with CD9 for the exosome marker and with Col1A1, fibronectin, osteocalcin, osteopontin, and proliferating cell nuclear antigen (PCNA) for the osteogenic-induced marker in triplicate for each condition. Briefly, 5 µg of protein samples from the exosomes and cell lysates were loaded onto an SDS-PAGE gel and transferred to a PVDF membrane. Thereafter, the membranes were blocked in 10 % bovine serum albumin with Tween-20 buffer at room temperature for 1 h and incubated with primary antibody diluent overnight at 4 °C. Horseradish peroxidase-linked secondary antibodies against rabbit (#7074, Cell Signaling Technology, USA) and mouse (#7076, Cell Signaling Technology, USA) were incubated for 2 h at room temperature. An ECL kit (Amersham Pharmacia Biotech, USA) was used to visualize the protein bands with a luminescent image analyzer (ImageQuant LAS 4000; GE Healthcare, USA).

## 2.5. In vivo assays

### 2.5.1. Subcutaneous implantation

Eighteen C57BL/6 mice were used in the experiments. Animals were randomly divided into 6 groups depending on which scaffolds were implanted; (1) PCL scaffold, (2) 10 % Ca-Si/PCL scaffold, (3) 20 % Ca-Si/PCL scaffold, (4) Exosome-coated PCL scaffold, (5) Exosome-coated 10 % Ca-Si/PCL scaffold, (6) Exosome-coated 20 % Ca-Si/PCL

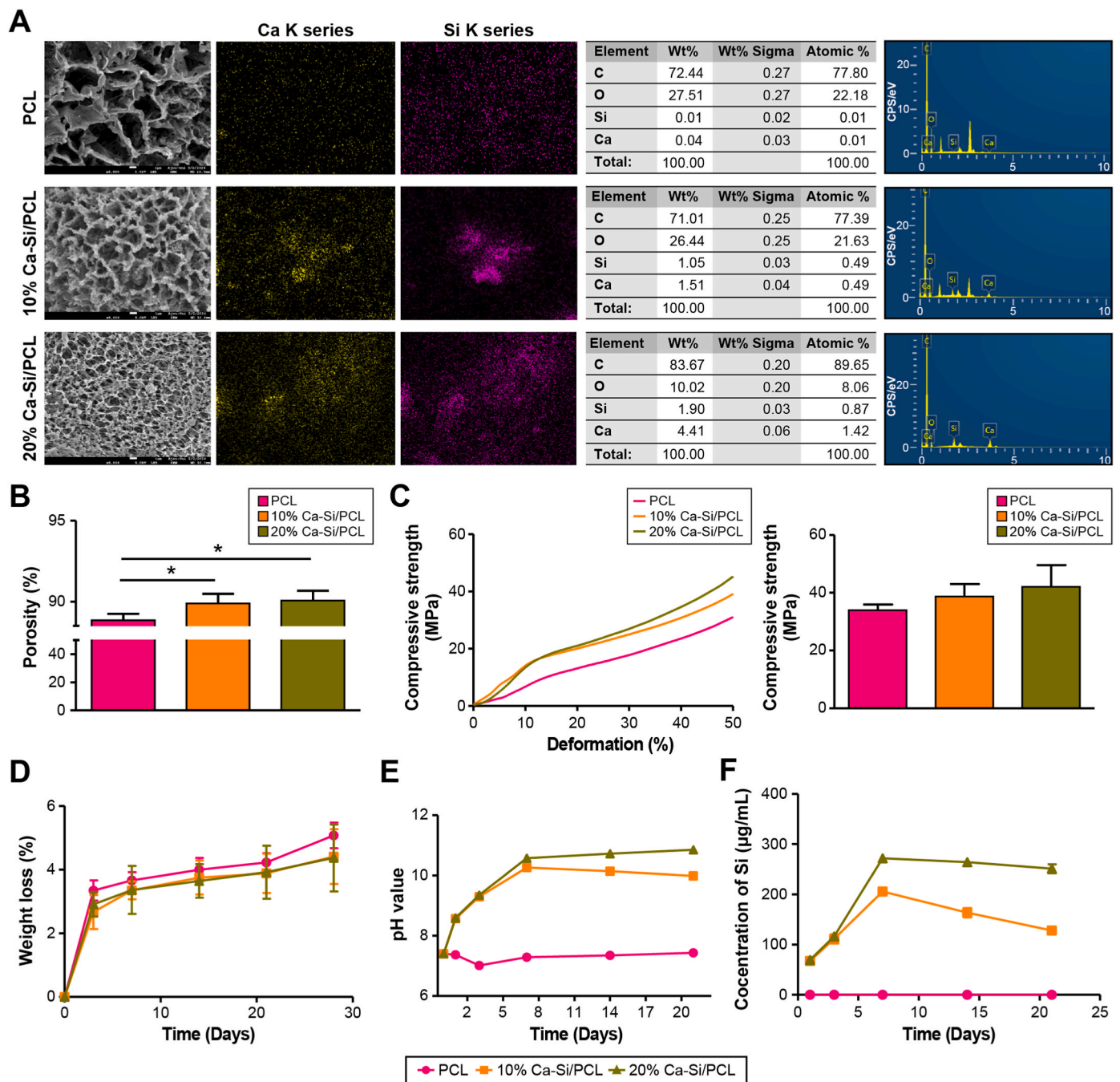


**Fig. 1.** Alterations of microstructures and mechanical and chemical properties of PCL and Ca-Si/PCL scaffolds. (A) SEM images and EDX mapping analyses of the PCL and Ca-Si/PCL scaffolds mixed with different concentrations of Ca-Si (10 % and 20 %). Magnification at  $5000\times$ , scale bar = 1  $\mu\text{m}$ , 5  $\mu\text{m}$ . (B) Porosity was calculated using volume and density. (C) Comprehensive strength increased as the concentration of Ca-Si was increased. (D) The weight loss of the scaffolds in a Tris-HCL solution was evaluated as the soaking time increased. Degradation initially occurred rapidly but then slowed. Ultimately, all scaffolds exhibited a weight loss of approximately 5 % over a period of 28 days. (E) PCL scaffold showed no effect on the pH value, but Ca-Si/PCL scaffolds became alkaline during degradation. (F) A graph of Si ion release in relation to scaffold degradation using ICP-OES. Continuous release of Si ions was detected as time passed in the Ca-Si/PCL scaffolds.  $*P < 0.05$ .

scaffold. The dorsal surgical area of 6-week-old C57BL/6 mice ( $n = 3$  per condition) was shaved and disinfected with ethanol. To implant the scaffold subcutaneously, a 1 cm transverse incision was made in the center of the shaved area. A pocket was formed in the skin using operating scissors, and then the scaffold was inserted and adjusted to ensure that it was not positioned within the incision. The wound was closed with 5-0 suture (polyamide, B. Braun, Germany). For analgesia, all mice were treated with Meloxicam (5 mg/kg, Meloxicam Oral Suspension, MWI Animal Health, Boise, ID) for 3 postoperative days. These

implanted scaffolds were sampled 7 days after implantation.

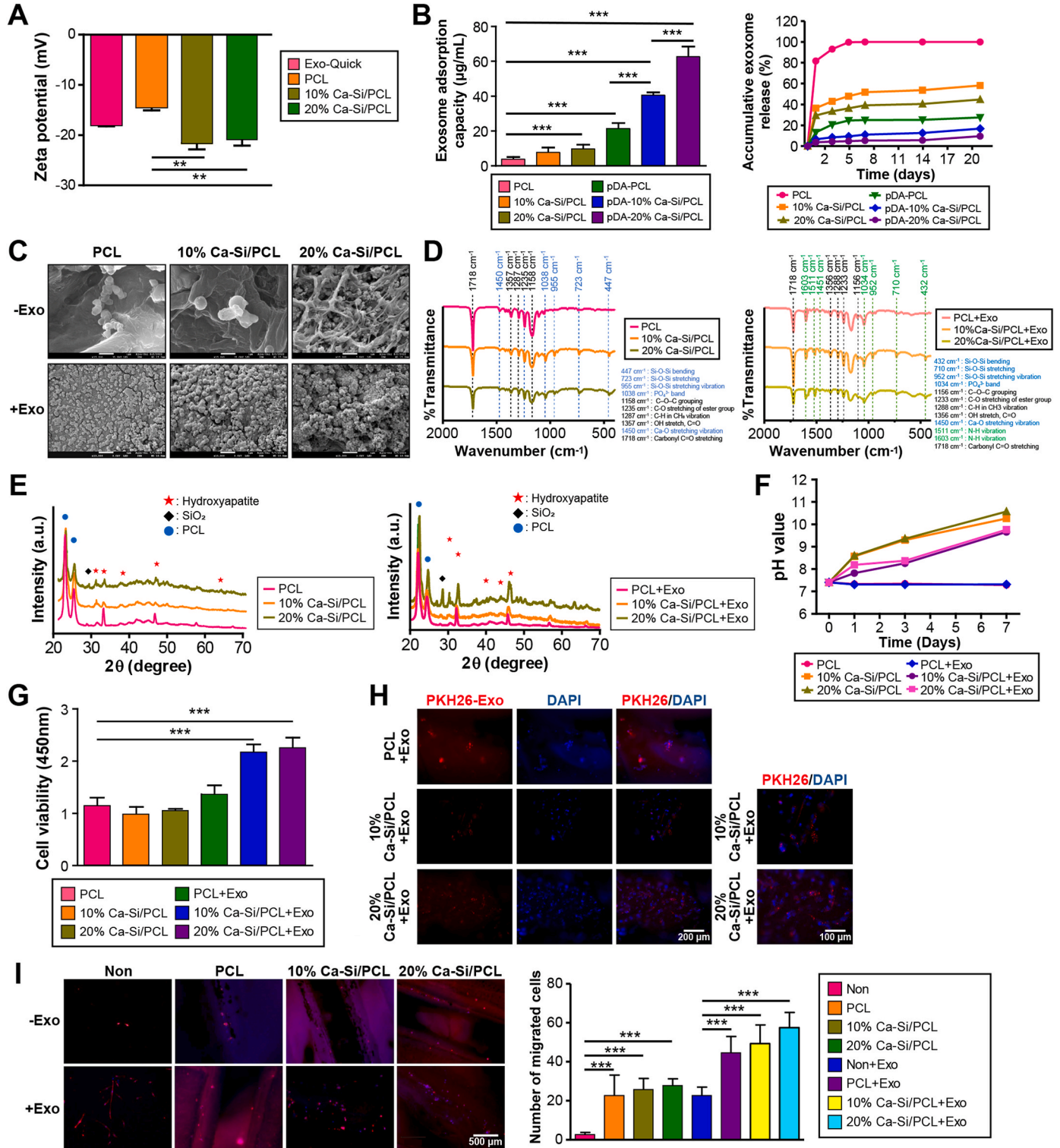
Hematoxylin & eosin (H&E) and immunofluorescence staining (CD44, Cell signaling, USA; CD73, Invitrogen, USA) were performed to identify mesenchymal stem cells. All tissue slides were captured using EVOS2 fluorescence microscopy, and the stained areas at similar locations were evaluated by Image J to identify cells that were positive around the scaffold.



2.5.2. Mouse calvarial defect model

Six weeks old Male C57BL6 mice were caged at  $22 \pm 1$  °C and  $55 \pm 5$  % humidity, on a 12-hrs light/dark auto-cycle, with food and water provided ad libitum. A total of 24 mice were used in this study, and they were divided into six groups, similar to the previous subcutaneous transplantation model, with four mice per group. Animals were anesthetized for calvarial defect surgery and the incision stie was shaved

with a razor. A midline incision was made over the calvaria skin using a scalpel, and the periosteum was gently dissected to expose the underlying bone. A 5 mm full-thickness circular defect was created using a hollow trephine bur attached to a low-speed dental drill. The defect was irrigated with sterilized normal saline. After defect formation was completed, the 3D fabricated scaffolds were implanted in the defect region. The incisions were closed with 5-0 polyamide suture (B. Braun,



(caption on next page)

**Fig. 2.** Differences in electrochemical properties, cell attachment, and mesenchymal stem cell recruitment of Ca-Si/PCL scaffolds in relation to exosome coating. (A) Exosome zeta potential was measured to indicate colloidal stability. The zeta potential of exosomes diluted in PBS ( $-17.84$  mV) and zeta potential of exosomes dispersed in PCL and 10 %, 20 % Ca-Si/PCL scaffolds ( $-14.40$ ,  $-21.63$ , and  $-20.79$ , respectively). (B) Ca-Si/PCL scaffolds treated with pDA showed a significant increase in exosome attachment. In exosome release profiles, the group containing Ca-Si exhibited a release amount  $<50$  %. Exosomes attached to surfaces coated with pDA exhibited a prolonged but lower level of release compared to the uncoated surfaces. (C) SEM images of scaffolds in the presence of Ca-Si and exosome. Hydroxyapatite (HA) formation was markedly increased in the exosome-coated condition. The Ca/P ratio of HA was greater than 1 for the structures that contained Ca-Si. Magnification of  $15,000\times$ , scale bar =  $1\ \mu\text{m}$ . (D) Fourier-transform infrared spectra of PCL and Ca-Si/PCL scaffolds with and without an exosome coating. Several peaks at  $450\text{--}1450\ \text{cm}^{-1}$  represent chemical bonding with Si. The intensity of these peaks increased in the scaffolds that contained Ca-Si.  $\text{PO}_4^{3-}$  peaks, which are due to HA ( $\text{Ca}_{10}(\text{PO}_4)_6(\text{OH})_2$ ), appeared in all conditions. In the graphs on the right, the peaks at  $1603$  and  $1511\ \text{cm}^{-1}$  indicate the presence of amide bonding, confirming the exosome coating. (E) HA formation was observed with X-ray diffraction. The number and intensity of HA-specific peaks increased in the Ca-Si scaffolds regardless of the presences of an exosome coating. (F) pH profiles of the different scaffolds for 7 days. The scaffolds containing Ca-Si showed an increase in pH to  $>8$ . However, in the exosome-coated scaffolds, the pH was decreased by 1 compared to the uncoated group. (G) TMSC was cultured on exosome-coated scaffolds. Cell viability was significantly increased for the exosome-coated Ca-Si/PCL scaffolds. (H) The exosomes were stained with PKH26 (red). Cells attached along the exosomes, and the exosomes were internalized into the cells. Scale bar =  $200\ \mu\text{m}$ ,  $100\ \mu\text{m}$ . (I) The relationship with TMSC migration and exosome coating was observed using a Boyden chamber assay. The number of cells increased even in conditions without scaffolds. Additionally, an increase in cell migration was identified with increasing concentration of Ca-Si. Scale bar =  $500\ \mu\text{m}$   $**P < 0.01$ ,  $***P < 0.001$ . Exo: exosome, pDA: polydopamine.

Germany). For analgesia, all mice were treated with Meloxicam (5 mg/kg, Meloxicam Oral Suspension, MWI Animal Health, Boise, ID) for 3 postoperative days. To assess bone formation, animals were sacrificed and the calvaria were collected at 8 weeks post-surgery.

### 2.5.3. Micro-CT scanning analysis

Mouse calvaria samples ( $n = 3$  per condition) were fixed in 10 % buffered formalin for 24 h and then stored in 70 % ethanol for 24 h. Tissue samples were scanned with a Skyscan 1076 *in vivo*  $\mu\text{CT}$  scanner (Skyscan, Belgium) at 40 kV, 250  $\mu\text{A}$ , with voxel size of  $18\ \mu\text{m}$ , an exposure time of 2356 ms (average 3 times), a 1 mm aluminum filter, and a  $0.4^\circ$  rotation step. Images were reconstructed using NRecon software and analyzed with CTAnalyse software (Skyscan). A 3D region of interest (ROI) was defined around the defect site. Bone volume fraction (BV/TV), trabecular number (Tb.N), trabecular thickness (Tb.Th), and trabecular separation distance (Tb.Sp) were analyzed within the ROI.

### 2.6. Ethics approval and consent to participate

Animal care and experimental procedures adhered to the National Institutes of Health Guidelines for the Care and Use of Laboratory Animals. The protocols of this study received approval from the Committee for Ethics in Animal Experiments at Ajou University School of Medicine (Approval No. 2022-0021).

### 2.7. Statistical analysis

GraphPad Prism6 (GraphPad Software, Inc., USA) was used for statistical analysis of all experiments, followed by one-way ANOVA and Tukey's multiple comparison test.  $p$ -values  $<0.05$  were considered statistically significant. All data were expressed as mean  $\pm$  SD.

## 3. Results

### 3.1. Differences in microstructures, mechanical properties, and chemical properties between PCL and Ca-Si/PCL scaffolds

The microstructures of the PCL and Ca-Si/PCL scaffolds were investigated and compared using SEM. Notably, the pore size was significantly decreased by the addition and increased concentrations of Ca-Si. PCL-only scaffolds exhibited larger pores and lower porosity compared to the PCL scaffolds augmented with Ca-Si. The presence of C, O, Ca, and Si on the scaffold surface was confirmed through the EDX analysis, indicating that  $\text{CaSiO}_3$  was uniformly mixed in the scaffolds (Fig. 1A and B). The incorporation of Ca-Si also resulted in increased compressive strength (Fig. 1C). Scaffold degradation, assessed by weight loss in a Tris-HCl solution, initially displayed rapid degradation kinetics. However, after 3 days, the degradation rate gradually attenuated. Ultimately, all scaffolds exhibited a weight loss of approximately 5 % over

28 days, and the degradation of Ca-Si/PCL scaffolds showed no significant difference compared to the bare PCL scaffolds (Fig. 1D). Furthermore, the Ca-Si/PCL scaffolds exhibited alkalization during degradation, unlike the PCL scaffolds (Fig. 1E). Analysis with ICP-OES showed a continuous release of Si ions from the Ca-Si/PCL scaffolds (Fig. 1F). These results demonstrated that the presence of Ca-Si in 3D-fabricated scaffolds altered their microstructures and mechanical strength and induced high pH values and sustainable Si release.

### 3.2. Effect of exosomes on the electrochemical properties, cell attachment, and MSC recruitment of Ca-Si/PCL scaffolds

To minimize pH value changes and to improve the bioactive and osteoconductive attributes of the Ca-Si/PCL scaffolds, they were modified with pDA coating and exosomes were attached to these scaffolds. The zeta potential of the exosomes diluted in PBS was  $-17.84$  mV (Supplementary Fig. 1). In addition, when dispersed in the scaffold extract containing Ca-Si, the exosomes showed a more pronounced negative charge, confirming their stable dispersion in a colloidal state (Fig. 2A) [26–28]. Exosomes, which have a negative surface charge, could be electrostatically bound to the surface of the scaffold, which exhibited a positive charge during Ca-Si decomposition. The number of exosomes attached to the surface of the scaffold significantly increased with the concentration of incorporated Ca-Si. Additionally, a more prolonged release profile was observed in the scaffolds containing higher levels of Ca-Si (Fig. 2B). Given that HA constitutes a significant portion of the inorganic components in human bones, the scaffolds were immersed in simulated body fluid to facilitate the precipitation of HA onto the material surface [29]. Subsequent analysis of the composition of the HA was conducted using SEM and EDX. Abundant HA particles were observed within the pores of the scaffolds that contained Ca-Si. Especially under the conditions of exosome attachment, the formation of HA noticeably increased compared to the non-coating condition, and the density was very high. Notably, the 20 % Ca-Si/PCL scaffold-derived HA exhibited a Ca/P ratio most similar to that of natural bone HA (Fig. 2C, Supplementary Fig. 2A). FTIR spectroscopy revealed characteristic PCL peaks at  $1718$ ,  $1357$ ,  $1287$ , and  $1235\ \text{cm}^{-1}$ , as well as HA-associated peaks at  $1038$  and  $1158\ \text{cm}^{-1}$  in all scaffolds. Distinct peaks indicating Si-related chemical bonding were exclusively discernible in the scaffolds that contained Ca-Si. Exosome-coated scaffolds also showed peaks at  $1603$  and  $1511\ \text{cm}^{-1}$ , indicating amide bonding and confirming strong exosome attachment (Fig. 2D). Analysis with XRD revealed an increase in the intensity of HA-specific peaks with higher concentrations of Ca-Si and the presence of exosomes (Fig. 2E). The changes in pH values were measured for 7 days. The pH of scaffolds with Ca-Si increased to  $>8$ , whereas that in scaffolds coated with exosomes was  $\sim 1$  unit lower than in the uncoated group (Fig. 2F, Supplementary Fig. 2B).

Next, TMSCs were cultured on the different scaffolds, and exosome

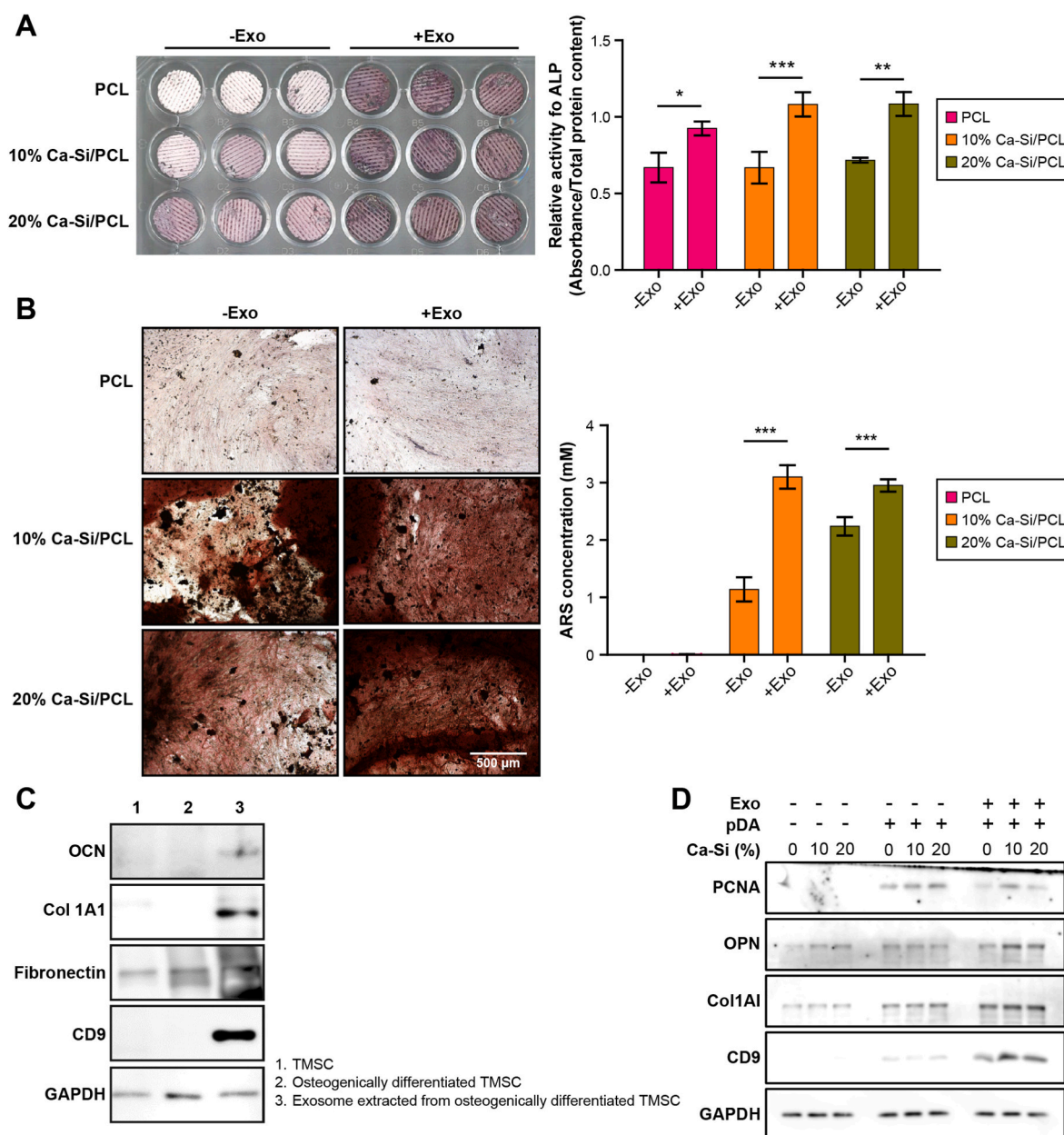


**Fig. 3.** Efficacy of Ca-Si and exosomes in osteogenic differentiation.

(A) TMSCs were cultured with an osteogenic differentiation medium on 3D-fabricated Ca-Si/PCL scaffolds for 7 days. ALP activity was enhanced in exosome-coated scaffolds compared to the noncoated scaffolds. Among the exosome-coated groups, higher ALP activity was observed in the scaffolds containing Ca-Si. (B) The TMSCs were cultured in the same conditions for 14 days, and red-stained cells were observed in the Ca-Si/PCL scaffolds, particularly in the presence of exosomes. (C) The results of western blot analysis showed that the expression of ECM proteins (Col1A1, fibronectin) and osteocalcin tended to increase in the exosomes extracted from osteogenically differentiated TMSCs. (D) Collagen synthesis, osteogenic differentiation, and proliferation were increased in the both exosome and pDA-coated Ca-Si scaffolds. \* $P < 0.05$ , \*\* $P < 0.01$ , \*\*\* $P < 0.001$ . Exo: exosome, ALP: Alkaline phosphatase, ARS: Alizarin Red S, OCN: Osteocalcin, PCNA: Proliferating cell nuclear antigen, OPN: Osteopontin.

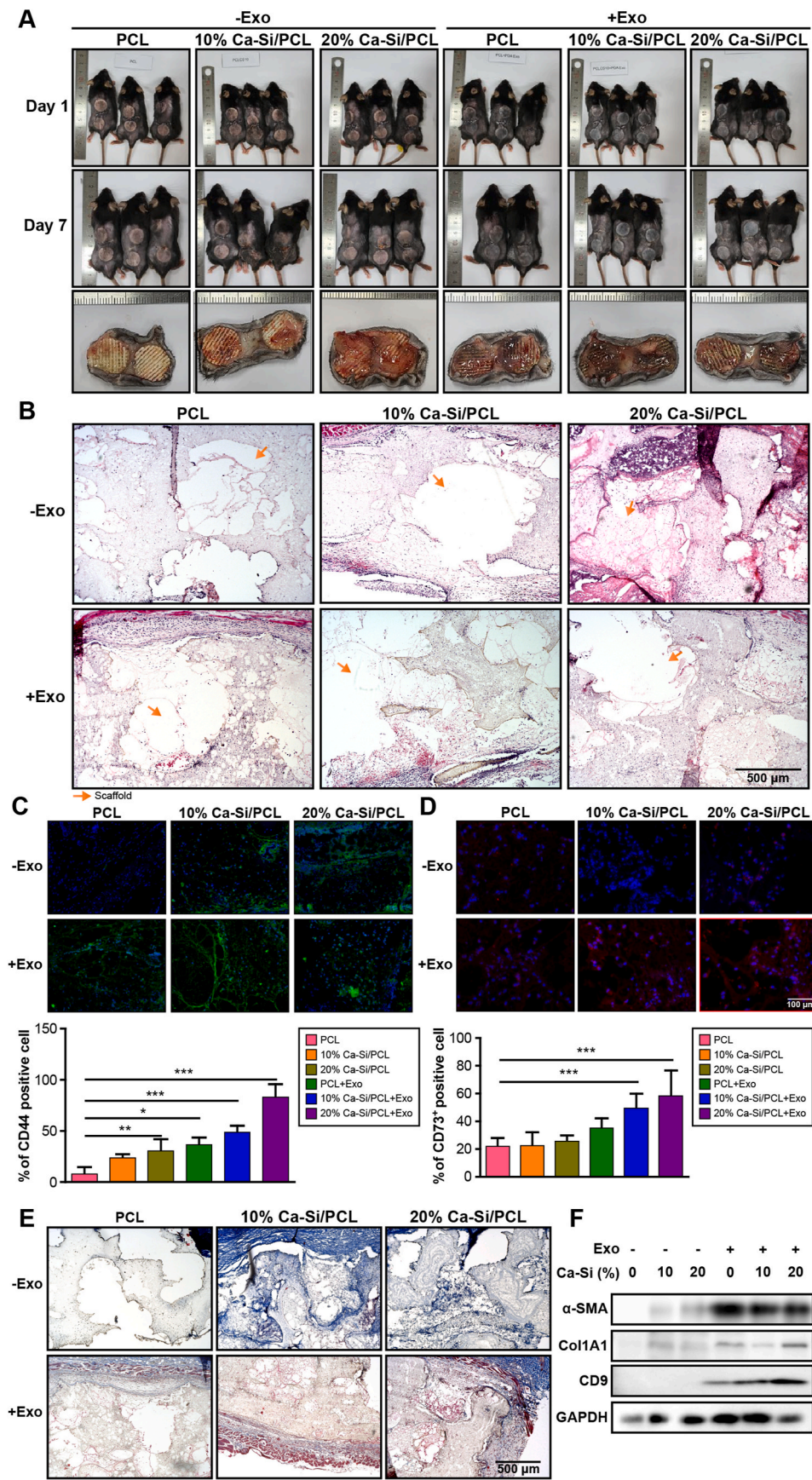
uptake was evaluated using PHK26 staining. First, we conducted experiments to identify the stemness and osteogenic differentiation of TMSCs (Supplementary Fig. 3). We observed a significant increase in cell viability in exosome-coated Ca-Si/PCL scaffolds compared to the scaffolds that were not coated with exosomes (Fig. 2G, Supplementary Fig. 2C). Merging PHK26 and DAPI staining highlighted the interactions between exosomes and cells. Confocal microscopy revealed that the TMSCs (DAPI, blue dots) were co-localized along the immobilized exosomes on the scaffolds (PHK26, red dots), with the number of exosomes increasing as the Ca-Si concentration increased (Fig. 2H, left columns). The successful internalization of exosomes into the attached TMSCs was confirmed in magnified images (Fig. 2H, right columns). The Boyden

chamber assay demonstrated a significant increase in migrated cells in the exosome-coated group and the group with higher Ca-Si concentrations (Fig. 2I, Supplementary Figs. 2D and 2E). Together, these data demonstrate that exosomes attachment and MSC recruitment in the exosome-coated Ca-Si/PCL scaffolds.

### 3.3. Enhanced osteogenic differentiation of TMSCs on exosome-coated Ca-Si/PCL scaffolds

Building on the observed exosome-mediated cell attachment, we evaluated osteogenic differentiation using ALP and ARS staining after culturing TMSCs in osteogenic differentiation medium for 7 or 14 days.





(caption on next page)



**Fig. 4.** The biocompatibility of exosome-coated Ca-Si/PCL scaffolds transplanted into the mouse subcutaneous region.

(A) Scaffolds transplanted into the subcutaneous region of mice were sampled after 7 days. (B) H&E staining. The quantity of infiltrated cells and tissues increased in the scaffolds that contained Ca-Si and were treated with exosomes. Scale bar = 500  $\mu$ m. (C, D) Immunocytochemistry with CD44 and CD73 revealed an increase in MSCs depending on the presence or absence of Ca-Si and exosomes. Blue: DAPI; green: CD44; red: CD73. Scale bar = 100  $\mu$ m. (E) Masson's trichrome staining. ECM synthesis was enhanced in the exosome-coated Ca-Si/PCL scaffolds. Scale bar = 500  $\mu$ m. (F) Increased  $\alpha$ -SMA and Col1A1 were noted in exosome-coated scaffolds through western blot analysis. \* $P < 0.05$ , \*\* $P < 0.01$ , \*\*\* $P < 0.001$ . Exo: exosome, SMA: Smooth muscle actin.

Higher ALP activity was observed in the scaffolds containing exosomes, especially for the 10 % and 20 % Ca-Si mass concentrations (Fig. 3A). Calcium deposition was pronounced in the Ca-Si-inclusive conditions, especially when combined with exosomes (Fig. 3B). Western blot analysis revealed that exosomes extracted from osteogenically differentiated expressed higher levels of ECM proteins (Col1A1, fibronectin) and the osteogenic marker osteocalcin compared to TMSCs or osteogenically differentiated TMSCs themselves (Fig. 3C). Additionally, increased expression of Col1A1, the early osteogenic differentiation marker osteopontin, and the proliferation marker PCNA was observed in the exosome-coated scaffolds (Fig. 3D). Based on these results, exosome-coated Ca-Si/PCL scaffolds demonstrated enhanced osteoconductivity and bioactivity.

### 3.4. Enhanced biocompatibility and tissue regeneration of exosome-coated Ca-Si/PCL scaffolds

To assess the *in vivo* biocompatibility and tissue regeneration, we transplanted the exosome-coated Ca-Si/PCL scaffolds into the subcutaneous region of mice and extracted them 7 days after transplantation (Fig. 4A). Histologic staining was used to observe enhanced *in situ* cell infiltration and ECM synthesis in the presence of exosomes and higher concentrations of Ca-Si (Fig. 4B–E). Additionally, immunocytochemistry using MSC markers (CD44 and CD73) revealed increased recruitment of MSCs with inclusion of the exosomes and Ca-Si (Fig. 4C and D). Western blot analysis of the tissues confirmed that fibrous tissue markers  $\alpha$ -SMA and ColA were significantly elevated in the exosome-coated condition (Fig. 4F).

### 3.5. Promotion of osteogenesis with exosome-coated Ca-Si/PCL scaffolds in calvarial defects

We created a 5-mm-diameter hole in the calvaria of BL6 mice and implanted a scaffold into the defect (Fig. 5A). After an 8-week period, the mice were sacrificed to evaluate bone formation. Cross-sectional slices from a micro-CT analysis showed minimal bone formation over the 8-week period in the group without exosomes, while the group with exosomes displayed bone tissue formation beginning from the scaffold edges and progressing inward. Notably, the inclusion of 10 % Ca-Si resulted in most of the scaffold area being filled with bone tissue (Fig. 5B). We analyzed the micro-CT results for trabecular separation, trabecular thickness, trabecular number, and the ratio of bone volume to tissue volume. A narrower trabecular separation suggests improved bone formation, greater trabecular thickness indicates increased strength, and a larger trabecular number implies greater density. All indicators demonstrated the superiority of the exosome-coated 10 % Ca-Si/PCL scaffold compared to the other scaffolds (Fig. 5C). H&E and Masson's trichrome staining showed increased bone formation, connective tissue growth, and angiogenesis in exosome-coated scaffolds, particularly in the exosome-coated 10 % Ca-Si/PCL scaffold (Fig. 5D and E). Immunofluorescence and western blot analysis revealed increased expression of osteoblast differentiation markers (Col1A1, OCN) and activation of the PI3K/AKT/mTOR pathway in the exosome-coated 10 % Ca-Si/PCL scaffold (Fig. 5F and G).

## 4. Discussion

Every year, more than 20 million patients globally encounter the

challenging issue of bone tissue loss caused by a variety of factors, including traumatic injuries and diseases such as osteopenia, osteoporosis, and severe dental conditions. The estimated cost of addressing these bone defects continues to increase each year [30]. Currently, the gold standard for bone graft materials is autogenous bone graft due to its impressive osteogenic properties. Nonetheless, the practical use of autogenous grafts is hindered by the need for extra surgical procedures to extract graft materials. This contributes to prolonged surgical durations, increased blood loss, and the potential for complications at the donor site [5,6]. Therefore, extensive research is currently underway to explore alternative biomaterials for bone substitutes.

These biomaterials must possess specific attributes to effectively function as substitutes for natural bone tissue. First, they should mimic the structural properties of native bone, including aspects such as porosity and mechanical characteristics. Moreover, biocompatibility is essential to ensure that the biomaterial interacts with biological systems without eliciting adverse reactions [31]. Biodegradability allows the biomaterial to gradually degrade as new bone forms, supporting the healing process. Additionally, the osteoconductivity and osteoinductivity of the biomaterial play crucial roles in its integration with the host tissue, fostering efficient bone healing and regeneration [5,6,30]. Here, we suggest a new osteogenic platform of exosome-coated Ca-Si/PCL composite graft.

A 3D-fabricated Ca-Si scaffold immersed in PCL solution was coated with exosomes. The *in vitro* study confirmed increased porosity, mechanical strength, and natural HA formation with the Ca/P ratio on the scaffold. The number of exosomes attached to the scaffold significantly increased with incorporation of Ca-Si. The release of exosomes from the scaffold was more sustainably controlled in the Ca-Si group compared to the bare PCL. The scaffold coated with exosomes exhibited excellent cell attachment and osteogenic differentiation, suggesting that the Ca-Si/PCL scaffold and exosomes have a synergistic efficacy. The attachment of exosomes significantly enhanced the biocompatibility of the scaffold and the *in situ* recruitment of stem cells when transplanted into the subcutaneous tissue of mice. The bone-regenerating efficacy of the scaffold with attached exosomes was confirmed using a mouse calvarial bone defect animal model.

Exosomes have attracted attention as a potential therapeutic option for repairing bone defects because of their ability to promote osteogenesis and osteogenic differentiation. Zhai et al. have reported that human MSC-derived exosomes can activate the PI3K/AKT signaling pathways by upregulating osteogenic miRNAs or downregulating anti-osteogenic miRNAs [32]. Consistent with previous report, the expression of osteoblast differentiation markers such as ColA1 and osteocalcin is increased, and the components of the PI3K/AKT pathway are upregulated in our Western blot and immunofluorescence assay [33]. However, exosomes have technical issues that need to be addressed before clinical application, such as limited retention stability and targeting efficiency [34]. Our highly porous 3D-fabricated Ca-Si/PCL scaffolds improve the efficiency of exosome targeting, facilitating consistent spacing and stable dispersion of the exosomes. With the 3D-fabricated Ca-Si/PCL scaffolds, exosomes can be delivered and distributed into a 3D-shaped bone defect, sustainably released into the body, and eventually create a favorable environment for bone regeneration by recruiting endogenous MSCs.

It seems that exosomes also influence the creation of a pH environment suitable for bone regeneration. The Ca-Si scaffold produces a bone-like apatite layer by generating HA in the body. During this process,





**Fig. 5.** Osteogenesis of exosome-coated Ca-Si/PCL scaffolds in the calvarial defect of mice.

(A) A 5-mm-diameter defect was created in the calvaria of BL6 mice, and a scaffold was inserted into the defect. The mice were sacrificed after 8 weeks. (B) Micro-CT images. In the 2D cross-sectional imaging slices, there was minimal bone formation in the group without exosomes. However, a pattern of bone formation was observed starting from the scaffold edges and progressing inward in the exosome-coated groups, especially in the exosome-coated 10 % Ca-Si/PCL scaffold. (C) Micro-CT analysis. The exosome-coated 10 % Ca-Si/PCL scaffold was superior to other scaffolds based on trabecular separation, trabecular thickness, trabecular number, and the ratio of bone volume to tissue volume. (D, E) H&E and Masson's trichome staining showed increased new bone formation and connective tissue, along with angiogenesis in the exosome-coated group, particularly in the exosome-coated 10 % Ca-Si/PCL scaffold. Scale bar = 200  $\mu\text{m}$ . (F) Osteocalcin was highly expressed in exosome-coated groups in the immunofluorescence assay. Scale bar = 200  $\mu\text{m}$ . (G) The expression of osteoblast differentiation markers (Col1A1, OCN) and PI3K/AKT/mTOR pathway components was increased in the western blot assay. Exo: Exosome, BV/TV: Bone volume/tissue volume, OCN: Osteocalcin.

$\text{Ca}^{2+}$  ions are released from the surface of the Ca-Si ceramic and exchanged with  $\text{H}^{+}$  ions in body fluid, leading to an increase in pH level [9]. Extracellular pH is one of the most important factors for regulating osteoblastic activities [35]. Osteoblastic differentiation and mineralization are accelerated under alkaline conditions, leading to enhanced bone regeneration [36]. However, extreme alkaline or acidic conditions outside the pH range of 6.5–10.5 result in poor cell viability and cell proliferation [37]. Our data show that the Ca-Si/PCL scaffold induces a high alkaline environment (pH > 10) during degradation. In contrast, coating with an exosome decreases the pH values by  $\sim 1$ . The decrease in pH enhances the survival and osteogenic properties of the recruited MSCs and increases the activities of bone regeneration-related proteins.

The strong electrostatic interaction between exosomes, which express negative zeta potentials, and the positively charged surface of scaffolds might be closely related to the stability of scaffolds. Isolated exosomes typically exhibit zeta potentials ranging from  $-6$  to  $-30$  mV, with values below  $-20$  mV indicating high colloidal stability [38]. Basic conditions increase exosome surface negativity by deprotonating the surface groups [39]. In our study, the zeta potentials of exosomes become more negative upon Ca-Si inclusion compared to PBS ( $-14.4$  mV) due to the alkaline pH of the Ca-Si solution during degradation. During apatite formation, highly porous 3D-fabricated Ca-Si/PCL scaffolds develop a negatively charged surface as they degrade. Afterward,  $\text{Ca}^{2+}$  ions in the body fluids attach to the negatively charged surface of the scaffolds, followed by attachment of  $\text{PO}_4^{3-}$  or  $\text{HPO}_4^{2-}$  [9]. Negatively charged exosomes also attach electrostatically to the positively charged, Ca-rich surface of the scaffold, like the  $\text{PO}_4^{3-}$  ions. This process is reinforced by the colloidal stability and more negative charge of the exosomes and the increase in the electrostatic attachment to the positively charged surface of the Ca-Si scaffold.

pDA coating was specifically incorporated into our new scaffolds to enhance the efficacy of the exosomes. pDA was investigated as a coating material to improve surface adhesion characteristics and chemical reactivity [40]. According to Lee et al. pDA coating significantly enhanced the adhesive ability of nanostructured polymer pillars. pDA, a natural mucin secreted by mussels, can adhere to any surface and form a coating layer through crosslinking polymerization [41,42]. This facilitates our pDA-coated scaffolds in increasing the local exosome concentration, prolonging the sustained release of exosomes, and maintaining mechanical strength by decreasing the degradation rate, which alleviates the high alkaline condition [43]. Additionally, the zeta potential of pDA-coated exosomes showed further negative charge, attributed to the catechol groups in pDA. This increased negative charge might strengthen the electrostatic attachment to the positively charged surface of the Ca-Si/PCL scaffold. Some studies reported that pDA coating promotes the osteogenic differentiation of stem cells [44,45]. Consistent with previous research, the number of migrated TMSCs increased and the capability of osteogenic differentiation and proliferation was elevated under pDA coating conditions. This suggests that pDA-coated scaffolds improved stem cell affinity by making the scaffold surface rougher, thereby enhancing stem cell attachment [42].

In this study, the *in vivo* results showed that the exosome-coated 10 % Ca-Si/PCL scaffold had the best bone regeneration effect contrary to the *in vitro* results. It seems to be a conundrum in the field of regenerative medicine that the challenges observed at the *in vitro* cellular level do not directly correlate with *in vivo* efficacy. The discrepancies between *in vitro*

and *in vivo* results may arise due the limitations of *in vitro* culture conditions, the complexity of the *in vivo* microenvironment, and various biological responses caused by the high Si content. This study is a proof-of-concept type of research, and further studies will be necessary to determine the optimal Ca-Si concentration and exosome composition for clinical applications.

## 5. Conclusion

In conclusion, our novel 3D-fabricated Ca-Si scaffolds, immersed in PCL and coated with exosomes, demonstrate superior bone regeneration effects. When these scaffolds are transplanted into a calvarial defect, they recruit MSCs and stimulate osteogenic differentiation, leading to bone regeneration. During bone regeneration, exosomes promoted cell proliferation, cell migration, and vascular formation, playing a significant role in tissue regeneration within the Ca-Si/PCL scaffold. Although further experiments are necessary to determine the optimal conditions, such as the concentration of Ca-Si, required for scaffold formation and to maximize the bone regeneration effects, this study demonstrates the potential clinical application of exosome-coated 3D-fabricated Ca-Si/PCL composite grafts as a platform for bone regeneration.

## CRedit authorship contribution statement

**Ju Hyun Yun:** Writing – original draft, Validation, Formal analysis, Conceptualization. **Hye-Young Lee:** Writing – original draft, Visualization, Methodology, Investigation, Conceptualization. **Se Hyun Yeou:** Writing – review & editing, Formal analysis. **Jeon Yeob Jang:** Writing – review & editing, Methodology. **Chul-Ho Kim:** Writing – review & editing, Methodology, Conceptualization. **Yoo Seob Shin:** Writing – review & editing, Supervision, Project administration, Methodology, Funding acquisition, Conceptualization. **Darryl D. D'Lima:** Writing – review & editing, Supervision, Project administration.

## Declaration of competing interest

The authors declare that they have no known competing financial interests or personal relationships that could have appeared to influence the work reported in this paper.

## Data availability

Data will be made available on request.

## Acknowledgments

This work was supported by the Basic Science Research Program through the National Research Foundation of Korea (NRF) funded by the Ministry of Education, Science, and Technology, Republic of Korea (NRF-2018R1D1A1A02043691), a grant of the Korea Health Technology R&D Project through the Korea Health Industry Development Institute (KHIDI), funded by the Ministry of Health & Welfare, Republic of Korea (HR21C1003).

## Appendix A. Supplementary data

Supplementary data to this article can be found online at <https://doi.org/10.1016/j.mtbio.2024.101283>.

## References

- [1] I.U.D. Osseo, The Critical Sized Bone Defect: Morphological Study of Bone Healing Studio Morfologico Della Riparazione Ossea, *Ann. Fac. Medic. Vet. di Parma XXVI* (2006) 97–110.
- [2] E.H. Schemitsch, Size matters: defining critical in bone defect size, *J. Orthop. Trauma* 31 (Suppl 5) (2017) S20–S22, <https://doi.org/10.1097/bot.0000000000000978>.
- [3] L.S. Bertol, R. Schabbach, L.A. Loureiro Dos Santos, Different post-processing conditions for 3D bioprinted  $\alpha$ -tricalcium phosphate scaffolds, *J. Mater. Sci. Mater. Med.* 28 (2017) 168, <https://doi.org/10.1007/s10856-017-5989-1>.
- [4] C. Deng, R. Lin, M. Zhang, C. Qin, Q. Yao, L. Wang, J. Chang, C. Wu, Micro/nanometer-structured scaffolds for regeneration of both cartilage and subchondral bone, *Adv. Funct. Mater.* 29 (2019) 1806068.
- [5] A.H. Schmidt, Autologous bone graft: is it still the gold standard? *Injury* 52 (Suppl 2) (2021) S18–S22, <https://doi.org/10.1016/j.injury.2021.01.043>.
- [6] H.S. Sohn, J.K. Oh, Review of bone graft and bone substitutes with an emphasis on fracture surgeries, *Biomater. Res.* 23 (2019) 9, <https://doi.org/10.1186/s40824-019-0157-y>.
- [7] W.R. Moore, S.E. Graves, G.I. Bain, Synthetic bone graft substitutes, *ANZ J. Surg.* 71 (2001) 354–361.
- [8] R.A. Youness, D.M. Tag El-deen, M.A. Taha, A review on calcium silicate ceramics: properties, limitations, and solutions for their use in biomedical applications, *Silicon* 15 (2023) 2493–2505.
- [9] P. Srinath, P. Abdul Azeem, K. Venugopal Reddy, Review on calcium silicate-based bioceramics in bone tissue engineering, *Int. J. Appl. Ceram. Technol.* 17 (2020) 2450–2464.
- [10] K. Liu, J. Wang, S. Fang, H. Wang, Y. Bai, Z. Zhao, Q. Zhu, C. Wang, G. Chen, H. Jiang, Effect of polycaprolactone impregnation on the properties of calcium silicate scaffolds fabricated by 3D printing, *Mater. Des.* 220 (2022) 110856.
- [11] Y.-H. Lin, Y.-C. Chiu, Y.-F. Shen, Y.-H.A. Wu, M.-Y. Shie, Bioactive calcium silicate/poly- $\epsilon$ -caprolactone composite scaffolds 3D printed under mild conditions for bone tissue engineering, *J. Mater. Sci. Mater. Med.* 29 (2018) 1–13.
- [12] Y. Lu, Z. Mai, L. Cui, X. Zhao, Engineering exosomes and biomaterial-assisted exosomes as therapeutic carriers for bone regeneration, *Stem Cell Res. Ther.* 14 (2023) 55.
- [13] Y. Zhang, Y. Liu, H. Liu, W.H. Tang, Exosomes: biogenesis, biologic function and clinical potential, *Cell Biosci.* 9 (2019) 1–18.
- [14] F. Tan, X. Li, Z. Wang, J. Li, K. Shahzad, J. Zheng, Clinical applications of stem cell-derived exosomes, *Signal Transduct. Targeted Ther.* 9 (2024) 17.
- [15] M. Ijaz, B. Aslam, I. Hasan, Z. Ullah, S. Roy, B. Guo, Cell membrane-coated biomimetic nanomedicines: productive cancer theranostic tools, *Biomater. Sci.* 12 (4) (2024) 863–895.
- [16] Y. Qin, J. Guan, C. Zhang, Mesenchymal stem cells: mechanisms and role in bone regeneration, *Postgrad. Med.* 90 (2014) 643–647.
- [17] S. Nikfarjam, J. Rezaie, N.M. Zolbanin, R. Jafari, Mesenchymal stem cell derived-exosomes: a modern approach in translational medicine, *J. Transl. Med.* 18 (2020) 1–21.
- [18] J. Wang, Y. Liu, F. Liu, S. Gan, S. Roy, I. Hasan, B. Zhang, B. Guo, Emerging extracellular vesicle-based carriers for glioblastoma diagnosis and therapy, *Nanoscale* 15 (2023) 10904–10938.
- [19] Y.J. No, J.J. Li, H. Zreiqat, Doped calcium silicate ceramics: a new class of candidates for synthetic bone substitutes, *Materials* 10 (2017) 153.
- [20] M. Li, H. Ma, F. Han, D. Zhai, B. Zhang, Y. Sun, T. Li, L. Chen, C. Wu, Microbially catalyzed biomaterials for bone regeneration, *Adv. Mater.* 33 (2021) 2104829.
- [21] H. Li, J. Chang, Stimulation of proangiogenesis by calcium silicate bioactive ceramic, *Acta Biomater.* 9 (2013) 5379–5389, <https://doi.org/10.1016/j.actbio.2012.10.019>.
- [22] Y. Huang, C. Wu, X. Zhang, J. Chang, K. Dai, Regulation of immune response by bioactive ions released from silicate bioceramics for bone regeneration, *Acta Biomater.* 66 (2018) 81–92.
- [23] H. Mohammadi, M. Hafezi, N. Nezafati, S. Heasarkhi, A. Nadernezhad, S. Ghazanfari, M. Sepantafar, Bioinorganic in bioactive calcium silicate ceramics for bone tissue repair: bioactivity and biological properties, *J. Ceram. Sci. Technol.* 5 (2014) 1–12.
- [24] C. Wu, Y. Ramaswamy, P. Boughton, H. Zreiqat, Improvement of mechanical and biological properties of porous CaSiO<sub>3</sub> scaffolds by poly (D, L-lactic acid) modification, *Acta Biomater.* 4 (2008) 343–353.
- [25] T. Zheng, L. Guo, Z. Du, H. Leng, Q. Cai, X. Yang, Bioceramic fibrous scaffolds built with calcium silicate/hydroxyapatite nanofibers showing advantages for bone regeneration, *Ceram. Int.* 47 (2021) 18920–18930.
- [26] J.-K. Lee, Surface charge effects on particulate retention by microporous membrane filters in liquid filtration, *Environmental Engineering Research* 3 (1998) 97–104.
- [27] T. Soares Martins, J. Catita, I. Martins Rosa, O. Ab da Cruz e Silva, A.G. Henriques, Exosome isolation from distinct biofluids using precipitation and column-based approaches, *PLoS One* 13 (2018) e0198820.
- [28] J. Kim, S. Li, S. Zhang, J. Wang, Plant-derived exosome-like nanoparticles and their therapeutic activities, *Asian J. Pharm. Sci.* 17 (2022) 53–69.
- [29] L. Wang, J. Wang, X. Zhou, J. Sun, B. Zhu, C. Duan, P. Chen, X. Guo, T. Zhang, H. Guo, A new self-healing hydrogel containing hucMSC-derived exosomes promotes bone regeneration, *Front. Bioeng. Biotechnol.* 8 (2020) 564731.
- [30] M.R. Iaquina, E. Mazzoni, M. Manfrini, A. D'Agostino, L. Trevisiol, R. Nocini, L. Trombelli, G. Barbanti-Brodano, F. Martini, M. Tognon, Innovative biomaterials for bone regrowth, *Int. J. Mol. Sci.* 20 (2019), <https://doi.org/10.3390/ijms20030618>.
- [31] B. Huzum, B. Puha, R.M. Necoara, S. Gheorghievici, G. Puha, A. Filip, P.D. Sirbu, O. Alexa, Biocompatibility assessment of biomaterials used in orthopedic devices: an overview, *Exp. Ther. Med.* 22 (2021) 1–9.
- [32] M. Zhai, Y. Zhu, M. Yang, C. Mao, Human mesenchymal stem cell derived exosomes enhance cell-free bone regeneration by altering their miRNAs profiles, *Adv. Sci.* 7 (2020) 2001334.
- [33] J. Zhang, X. Liu, H. Li, C. Chen, B. Hu, X. Niu, Q. Li, B. Zhao, Z. Xie, Y. Wang, Exosomes/tricalcium phosphate combination scaffolds can enhance bone regeneration by activating the PI3K/Akt signaling pathway, *Stem Cell Res. Ther.* 7 (2016) 136, <https://doi.org/10.1186/s13287-016-0391-3>.
- [34] S. Ma, Y. Zhang, S. Li, A. Li, Y. Li, D. Pei, Engineering exosomes for bone defect repair, *Front. Bioeng. Biotechnol.* 10 (2022) 1091360.
- [35] T.R. Arnett, Extracellular pH regulates bone cell function, *J. Nutr.* 138 (2008) 415S–418S.
- [36] A.-M. Galow, A. Rebl, D. Koczan, S.M. Bonk, W. Baumann, J. Gimsa, Increased osteoblast viability at alkaline pH in vitro provides a new perspective on bone regeneration, *Biochemistry and biophysics reports* 10 (2017) 17–25.
- [37] C.R. Kruse, M. Singh, S. Targosinski, I. Sinha, J.A. Sorensen, E. Eriksson, K. Nuutila, The effect of pH on cell viability, cell migration, cell proliferation, wound closure, and wound reepithelialization: in vitro and in vivo study, *Wound Repair Regen.* 25 (2017) 260–269.
- [38] J. Jang, H. Jeong, E. Jang, E. Kim, Y. Yoon, S. Jang, H.-S. Jeong, G. Jang, Isolation of high-purity and high-stability exosomes from ginseng, *Front. Plant Sci.* 13 (2023) 1064412.
- [39] G. Midekessa, K. Godakumara, J. Ord, J. Viil, F. Lattekivi, K. Dissanayake, S. Kopanchuk, A. Rincken, A. Andronowska, S. Bhattacharjee, Zeta potential of extracellular vesicles: toward understanding the attributes that determine colloidal stability, *ACS Omega* 5 (2020) 16701–16710.
- [40] D. Hauser, D. Septiadi, J. Turner, A. Petri-Fink, B. Rothen-Rutishauser, From bioinspired glue to medicine: polydopamine as a biomedical material, *Materials* 13 (2020) 1730.
- [41] H. Lee, B.P. Lee, P.B. Messersmith, A reversible wet/dry adhesive inspired by mussels and geckos, *Nature* 448 (2007) 338–341, <https://doi.org/10.1038/nature05968>.
- [42] Y. Zhou, G. Deng, H. She, F. Bai, B. Xiang, J. Zhou, S. Zhang, Polydopamine-coated biomimetic bone scaffolds loaded with exosomes promote osteogenic differentiation of BMSC and bone regeneration, *Regenerative Therapy* 23 (2023) 25–36.
- [43] C. Li, S.-Y. Liu, M. Zhang, W. Pi, B. Wang, Q.-C. Li, C.-F. Lu, P.-X. Zhang, Sustained release of exosomes loaded into polydopamine-modified chitin conduits promotes peripheral nerve regeneration in rats, *Neural Regeneration Research* 17 (2022) 2050–2057.
- [44] N.Y. Shim, J.S. Heo, Performance of the polydopamine-graphene oxide composite substrate in the osteogenic differentiation of mouse embryonic stem cells, *Int. J. Mol. Sci.* 22 (2021) 7323.
- [45] W. Li, Y. Liu, P. Zhang, Y. Tang, M. Zhou, W. Jiang, X. Zhang, G. Wu, Y. Zhou, Tissue-engineered bone immobilized with human adipose stem cells-derived exosomes promotes bone regeneration, *ACS Appl. Mater. Interfaces* 10 (2018) 5240–5254.